

ORIGINAL ARTICLE

Development and Emergence of Individual Variability in the Functional Connectivity Architecture of the Preterm Human Brain

Yuehua Xu^{1,2,3}, Miao Cao^{1,2,3}, Xuhong Liao^{1,2,3}, Mingrui Xia ^{1,2,3}, Xindi Wang^{1,2,3}, Tina Jeon⁴, Minhui Ouyang⁴, Lina Chalak⁵, Nancy Rollins⁶, Hao Huang^{4,7} and Yong He^{1,2,3}

¹National Key Laboratory of Cognitive Neuroscience and Learning, Beijing Normal University, Beijing 100875, China, ²Beijing Key Laboratory of Brain Imaging and Connectomics, Beijing Normal University, Beijing 100875 China, ³IDG/McGovern Institute for Brain Research, Beijing Normal University, Beijing 100875 China, ⁴Department of Radiology, Children's Hospital of Philadelphia, Philadelphia, PA 19104, USA, ⁵Department of Pediatrics, University of Texas Southwestern Medical Center, Dallas, TX 75390, USA, ⁶Department of Radiology, University of Texas Southwestern Medical Center, Dallas, TX 75390, USA and ⁷Department of Radiology, University of Pennsylvania, Philadelphia, PA 19104, USA

Address correspondence to Yong He, PhD, National Key Laboratory of Cognitive Neuroscience and Learning, Beijing Key Laboratory of Brain Imaging and Connectomics, IDG/McGovern Institute for Brain Research, Beijing Normal University, Beijing 100875, China. Email: yong.he@bnu.edu.cn; Hao Huang, PhD, Department of Radiology, Children's Hospital of Philadelphia, Perelman School of Medicine, University of Pennsylvania, Philadelphia, PA 19104, USA. Email: hao.huang@uphs.upenn.edu

Yuehua Xu and Miao Cao contributed equally to this work

Abstract

Individual variability in human brain networks underlies individual differences in cognition and behaviors. However, researchers have not conclusively determined when individual variability patterns of the brain networks emerge and how they develop in the early phase. Here, we employed resting-state functional MRI data and whole-brain functional connectivity analyses in 40 neonates aged around 31–42 postmenstrual weeks to characterize the spatial distribution and development modes of individual variability in the functional network architecture. We observed lower individual variability in primary sensorimotor and visual areas and higher variability in association regions at the third trimester, and these patterns are generally similar to those of adult brains. Different functional systems showed dramatic differences in the development of individual variability, with significant decreases in the sensorimotor network; decreasing trends in the visual, subcortical, and dorsal and ventral attention networks, and limited change in the default mode, frontoparietal and limbic networks. The patterns of individual variability were negatively correlated with the short- to middle-range connection strength/number and this distance constraint was significantly strengthened throughout development. Our findings highlight the development and emergence of individual variability in the functional architecture of the prenatal brain, which may lay network foundations for individual behavioral differences later in life.

Key words: connectome, functional connectivity, neonate, network, prenatal

Introduction

People differ in their thoughts and behaviors. These cognitive and behavioral differences mainly originate from individual variability in the structural and functional architectures of the brain (Kanai and Rees 2011). Using histological and neuroimaging techniques, researchers have revealed widespread individual variability in various structural and functional characteristics, including cortical morphology (Good et al. 2001; Hill et al. 2010), cytoarchitectonic mapping (Amunts et al. 2004, 2005), and task-evoked activation (Baldassarre et al. 2012; Frost and Goebel 2012). These brain variations across individuals may represent a joint outcome of complex gene-environment interactions (Hill et al. 2010; Petanjek et al. 2011; Chen et al. 2012; Gao et al. 2014; Wang and Liu 2014).

In recent years, researchers have increasingly focused on inter-subject variability in the functional connectivity architecture of the human brain. Specifically, with the progress achieved in the resting-state functional MRI (R-fMRI) technique, researchers have been able to non-invasively map the intrinsic functional connectivity patterns of the brain by measuring the correlations of spontaneous low-frequency fluctuations among regions (Biswal et al. 1995; Fox et al. 2005). A recent R-fMRI study of the healthy adult brain found that there was higher individual variability of functional connectivity in the heteromodal association cortices, in contrast to lower variability in the unimodal cortices (Mueller et al. 2013). This spatial pattern was quite similar to distant connectivity distributions, evolutionary cortical expansion, and hemispheric specialization (Mueller et al. 2013; Wang and Liu 2014). Moreover, heteromodal regions with higher variability underlie individual differences in higher-order cognitive functions (Baldassarre et al. 2012; Smith et al. 2013; Liu et al. 2017; Liao, Cao et al. 2017) and provide valuable information regarding the brain fingerprints responsible for identifying individuals (Finn et al. 2015; Airan et al. 2016; Shen et al. 2017; Liu et al. 2018). Interestingly, Gao et al. (2014) observed that individual variability patterns in the functional connectivity of healthy adult brains have emerged by the time of birth. Notably, studies of the brain connectivity architectures at a time point even earlier than full-term birth are crucial for obtaining a better understanding of the development and emergence of the individual variability patterns of brain networks before birth.

The third trimester of pregnancy represents a critical period of rapid neuronal growth and neural circuit establishment (Sidman and Rakic 1973; Rakic 1972, 1995). Specifically, a large number of neurons in the cortical plate are connected via cellular activities such as dendritic arborization, synapse formation and axonal growth (Molliver et al. 1973; Kostovic and Jovanov-Milosevic 2006; Bystron et al. 2008). These interconnected neurons are thought to foster the formation and differentiation of the neuronal circuits that underlie primary sensorimotor processing and higher cognitive functions (Dehaene-Lambertz and Spelke 2015). Several R-fMRI studies have shown dramatic changes in the functional connectivity architectures of the brain, including the rapid development of primary regions and prolonged development of higher-order regions (Fransson et al. 2007; Doria et al. 2010; Smyser et al. 2011; Cao, He et al. 2017), the medial-to lateral maturation of interhemispheric connectivity (Smyser et al. 2010; Thomason et al. 2013), and the increased subcortical-motor connectivity but decreased connectivity between the subcortical and heteromodal regions (Thomason et al. 2015; Toulmin et al. 2015). However, further studies are needed to elucidate whether the individual

variability patterns in the functional connectivity architecture of the human brain emerge in the third trimester of pregnancy and, if so, to further characterize how they develop during this critical prenatal phase.

To address these issues, in the present study, we employed R-fMRI data and voxel-wise whole-brain functional connectivity analysis to investigate the early development of individual variability in the human brain networks in 40 preterm and term infants aged 31.3–41.7 postmenstrual weeks at the time of the scan. We aimed to delineate both the spatial distributions and development patterns of individual variability during the third trimester. Specifically, we sought to determine (i) whether the spatial patterns of individual variability in the functional connectivity architecture previously observed in healthy adults, has already emerged during the prenatal phase; (ii) how the individual variability in functional connectivity develops over time during this critical period; and (iii) how the anatomical distances in the brain constrain the development of individual variability in the functional connectivity architecture.

Materials and Methods

Participants

Fifty-two normal preterm and term infants at postmenstrual ages ranging from 31.3 to 41.7 weeks at the time of the scan were included in the present study. These infants were recruited from Parkland Hospital in Dallas and selected after rigorous screening procedures, which were conducted by a neonatologist (L.C.) and an experienced pediatric neuroradiologist (N.R.) based on the infants' ultrasound and clinical MRI data as well as the infants' and mothers' medical records. Notably, ultrasound scans are routinely ordered and performed and the clinical MRI sequences included high-resolution (in-plane) T1-weighted, T2-weighted, and FLAIR (Fluid-Attenuated Inversion-Recovery) MRI. These infants were part of the cohort used to study normal prenatal and perinatal development in our previous studies (Yu et al. 2016; Cao, He et al. 2017; Ouyang et al. 2017; Feng et al. 2018). The exclusion criteria included evidence of bleeding or an intracranial abnormality by serial sonography; maternal drug or alcohol abuse during pregnancy; grade I–IV intraventricular hemorrhaging; hydrocephalus; germinal matrix hemorrhage; periventricular leukomalacia; hypoxic-ischemic encephalopathy; lung disease or bronchopulmonary dysplasia; body or heart malformations; chromosomal abnormalities; necrotizing enterocolitis requiring intestinal resection or complex feeding/nutritional disorders; defects or anomalies in the forebrain, brainstem or cerebellum; brain tissue dysplasia- or hypoplasia; abnormal meninges; alterations in the pial or ventricular surface; or white matter lesions. Written and informed parental consent was obtained from each infant's mother and/or father. This study was approved by the Institutional Review Board. Data from 12 infants were excluded from further analysis due to excessive head motion (see "Image Preprocessing"). Therefore, the R-fMRI data for the remaining 40 normal preterm and term infants (29 males) were subjected to further analysis. Table 1 presents the detailed demographic information of the infants.

Data Acquisition

All infants were scanned during natural sleep without sedation and were well-fed prior to the scan. Earplugs, earphones, and extra foam padding were applied to reduce the sound of the scanner while the neonates were asleep. Images were acquired

Table 1 Demographic information of the infants in the main data analysis

Number of infants	Birth or scan	Age range (weeks)	Weight range (kg)	Male, n(%)	White, n(%)	Mode of delivery ^a
40	At birth	25.1–40.7 (33.2 ± 4.5)	0.8–4.0 (2.1 ± 0.9)	29 (73)	30 (75)	C: 24 V: 16
40	At scan	31.3–41.7 (37.0 ± 2.7)	1.4–4.1 (2.6 ± 0.7)	29 (73)	30 (75)	C: 24 V: 16

Note: ^aC stands for C-section and V for vaginal birth. The feeding practice for all infants was breast-feeding.

using a Philips 3 T Achieva MR scanner with an 8-channel SENSE head coil at the Children’s Medical Center at Dallas. R-fMRI scans were obtained using a T2-weighted gradient-echo EPI sequence: repetition time = 1500 ms, echo time = 27 ms, flip angle = 80°, in-plane imaging resolution = 2.4 × 2.4 mm², in-plane field of view = 168 × 168 mm², slice thickness = 3 mm with no gap, and slice number = 30. Two hundred and ten whole-brain EPI volumes were acquired. A co-registered T2-weighted structural image was acquired with a turbo spin echo sequence: repetition time = 3000 ms, effective echo time = 80 ms, in-plane imaging resolution = 1.5 × 1.5 mm², in-plane field of view = 168 × 168 mm², slice thickness = 1.6 mm with no gap, and slice number = 65. The acquired T2-weighted image was zero-filled to a 256 × 256 image matrix.

Image Preprocessing

The R-fMRI images were preprocessed using Statistical Parametric Mapping (SPM8, <http://www.fil.ion.ucl.ac.uk/spm>) and Data Processing Assistant for Resting-State fMRI [DPARSF, (Yan and Zang 2010)]. The first 15 volumes were discarded to allow the signal to reach a steady state; thus, 195 time points remained for each infant. The remaining data were corrected for the acquisition time delay between slices and head motion between volumes. Here, the data from 12 infants were removed because of head-motion displacement >5 mm, rotation >5°, or a mean frame wise displacement (mFD) (Power et al. 2012) > 1 mm. The individual functional data were first co-registered to the corresponding high-resolution T2-weighted structural images using a linear transformation. The individual T2-weighted images were then non-linearly registered to a 37-week brain template (Serag et al. 2012). A customized template was generated by averaging the resulting normalized T2-weighted structural images of all infants and used for the second registration of individual T2-weighted images. The co-registered functional data were normalized to the custom-made template by applying the transformation parameters estimated during the second registration of T2-weighted images and resampled to 3 mm isotropic voxels. In addition, previously reported templates of the cortex, deep gray matter, white matter, and cerebrospinal fluid tissue templates recorded at 37 weeks (Serag et al. 2012) were also registered to the customized template to generate the gray matter mask. Next, the normalized functional imaging data were smoothed with a Gaussian kernel (full width at half-maximum of 4 mm) and temporally bandpass filtered (0.01–0.10 Hz). Finally, several nuisance variables, including Friston’s 24 head-motion parameters (Friston et al. 1996), and average signals from white matter and cerebrospinal fluid tissue were removed using a multivariate linear regression analysis to reduce the effects of non-neuronal signals. The resulting residuals were subjected to further analysis.

Individual Functional Connectivity Matrices

For each infant, we first calculated the Pearson correlation coefficients between the time series of all pairs of voxels within a

gray matter mask ($N_{\text{voxel}} = 7101$), which was predefined by thresholding the combined cortex and deep gray matter probability templates. Fisher’s *r*-to-*z* transformation was then performed to improve the normality of correlation coefficients. The absolute values of the correlation matrix were used in all subsequent analyses to retain the strength of both synchronous activity (positive correlation) and asynchronous activity (negative correlation) between pairs of voxels. Furthermore, the connectivity terminating within 10 mm of each voxel was set to zero to avoid potential sharing of signals between nearby voxels (Cao, He et al. 2017). For each infant, we obtained one 7101 × 7101 matrix that captured the basic functional connectivity architecture of the whole brain.

Individual Variability of Functional Connectivity

We performed the qualitative and quantitative analyses described below to examine the development of individual variability in the functional connectivity architecture (Fig. 1).

(i) *Sliding window analysis*: An across-subject sliding window analysis was performed for all infants in ascending order of age, with a fixed number of infants (here $M = 10$) and a step size of one (i.e., infants 1–10 in window 1, infants 2–11 in window 2... infants 31–40 in window 31). This method generated 31 overlapping subgroups of infants with window ages ranging from 33.4 weeks to 40.6 weeks. This approach allowed us to qualitatively examine *continuous* changes in individual variability patterns of functional connectivity with age across infants. For a given subgroup with M infants, we calculated the voxel-wise individual variability values for the functional connectivity architecture using the functional connectivity matrix obtained above. Specifically, the individual variability value of voxel i was defined as follows:

$$V_i = 1 - E[\text{corr}(F_i(S_p), F_i(S_q))] \quad (1)$$

where $p, q = 1, 2, \dots, M$ ($p \neq q$); M is the number of infants in the subgroup; and $F_i(S_p)$ is an N -length ($N_{\text{voxel}} = 7101$) vector of functional connectivity values of voxel i in infant p . The term *corr* calculates the correlation coefficients between any two functional connectivity profiles, which are then averaged to represent the similarity within M infants. This measurement of individual variability in functional connectivity has been recently used in adults and neonates (Mueller et al. 2013; Gao et al. 2014).

(ii) *Group-based statistical analysis*: We performed the analysis described below to quantify the significant differences in individual variability patterns among different age groups. Briefly, we first divided all infants into three groups of different age bins representing early preterm, preterm and term equivalents (Group 1: 31.3–35.3 weeks [$n = 14$]; Group 2: 35.6–38.4 weeks [$n = 12$]; and Group 3: 38.7–41.7 weeks [$n = 14$], respectively). This approach allowed us to perform *statistical* comparisons to evaluate age-related changes in individual variability patterns of functional connectivity. For each group, the individual variability of functional connectivity was computed using Equation (1). Notably, a

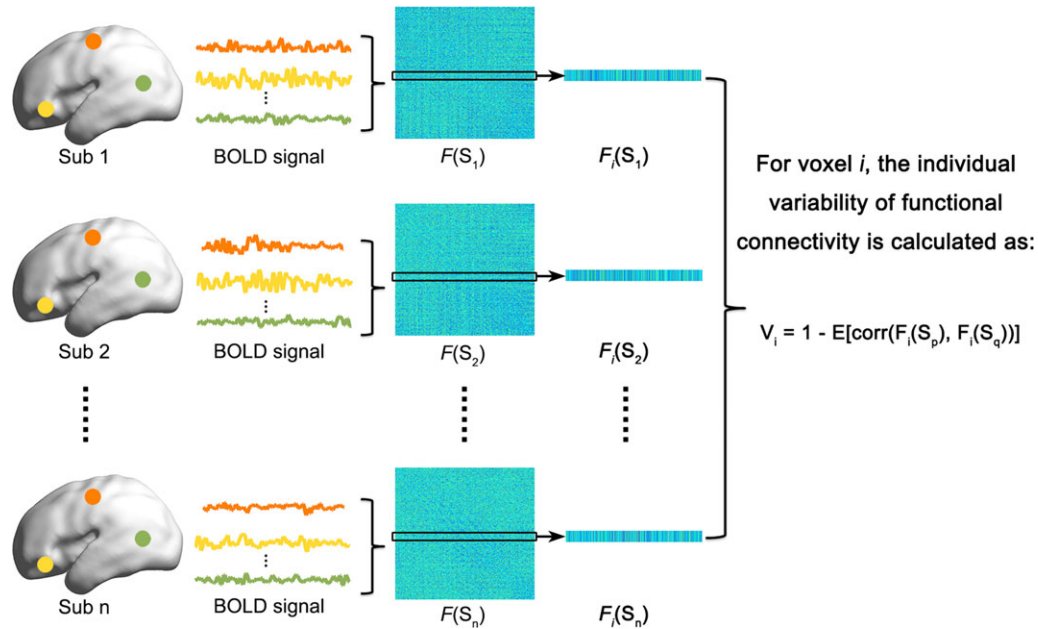


Figure 1. The flow chart of individual variability analysis of functional connectivity. For details, please see the Materials and Methods.

term group containing 10 infants born after 38 weeks was additionally selected as the control group for comparison (Term Group: 38.4–41.0 weeks [$n = 10$]). Furthermore, we also estimated the similarity of spatial patterns of individual variability between all 31 windows and the Term Group by calculating the Pearson correlation coefficients.

We employed a predefined functional parcellation atlas that was derived from 1000 healthy adults using a clustering approach (Yeo et al. 2011) to further examine whether individual variability in functional connectivity exhibited different developmental patterns across brain systems. The functional atlas of adult brains was transformed to the infant template space using non-linear registration. Because only cortical regions were included in this atlas, we also added a predefined subcortical mask for infants (Serag et al. 2012). Therefore, we obtained a customized parcellation atlas with eight brain systems: the visual, somatomotor, dorsal attention, ventral attention, limbic, frontoparietal, default mode, and subcortical systems. For each window/group, we calculated the mean variability values of all voxels within each system to represent the system-specific variability.

Individual Variability and Connection Distance

We further investigated whether the development of individual variability of functional connectivity was constrained by the anatomical distance. Specifically, all functional connections were divided into three bins according to their Euclidean distance, D_{ij} (which was considered an approximate anatomical distance): short-range (10–30 mm), middle-range (30–60 mm) and long-range distance (>60 mm). The connectivity numbers and strength for each distance bin were quantified for each voxel. Briefly, for each infant, the whole-brain functional connectivity matrix was first thresholded with a predefined $r = 0.2$ (here, r represents the correlation between blood oxygenation level-dependent signals, corresponding to the significance level at $P = 0.005$). Next, for a given voxel i , the connectivity number was calculated as the total number of remaining connections

to which each voxel was linked within every distance bin. The connectivity strength of voxel i within each bin was computed using the following equation:

$$S(i) = \frac{1}{N_{\text{voxel}} - 1} \sum_{j \neq i} |r_{ij}| \quad (2)$$

where $N_{\text{voxel}} = 7101$ and the distance between voxel i and j lies within the specific bin. Next, the values were averaged across infants to represent the mean connectivity number/strength at different distance bins for each age group. Finally, we computed across-voxel Pearson's correlation coefficients between the mean number/strength of the distance-dependent connections and individual variability maps.

Statistical Analysis

For the quantitative statistical analyses, we compared the variability values across different groups of infants using a non-parametric permutation approach (10 000 permutations) to identify significant developmental changes. Specifically, in each permutation, the infants in two groups (i.e., Group 1 vs. Group 2) were randomly reallocated to two new groups, and then an individual variability map was calculated for each newly generated group using Equation (1). After 10 000 permutations, a null distribution of group differences in variability values for each voxel was obtained for statistical comparisons. Moreover, we calculated the largest edge connected-components in the randomized group-difference maps to obtain the null distribution for a cluster size with 10 000 permutations. Significant correction for multiple comparisons was performed with $P < 0.01$ for voxels and $P < 0.05$ for the cluster size. Similarly, significant differences in the means and standard deviations of global and system-level variability values between different age groups were also determined using the permutation approach. Furthermore, the non-parametric Kruskal-Wallis H test was performed to estimate the differences in variability values across different systems within the same age group using SPSS 20.0 software (IBM Corp.,

Armonk, NY, USA), at a significance level of $P < 0.05$, with Bonferroni correction for multiple comparisons.

Validation Analysis

To evaluate the reliability of our findings, we examined the influences of different strategies and factors in the image preprocessing and the variability analysis. The validation analyses are described in detail below.

For the image preprocessing steps, we evaluated the influences of different brain templates during spatial normalization, global signal removal and head motion. (1) In our main analysis, all infants were registered to a 37-week template, which might induce anatomical bias due to up-registering immature brains to the older template. To address this issue, we conducted an additional region-wise analysis (46 regions of interest (Makropoulos et al. 2016)) using the age-specific templates (Serag et al. 2012) for each infant during normalization. Given that the regional atlas of infants was too coarse for detailed information detection, we also conducted a voxel-level analysis using the age-specific template of each window/group during normalization. (2) Given the debatable application of global signal removal in analyses of the whole-brain network during R-fMRI data processing (Murphy and Fox 2017), we used the data without performing the global signal regression in the main analysis. In addition, we also evaluated our results using data from which the global signal was removed because several studies suggested that this procedure might partially reduce the influences of non-neuronal signals (Satterthwaite et al. 2013; Power et al. 2014, 2017). (3) In our main analysis, we excluded the data from infants with head-motion displacement >5 mm, rotation $>5^\circ$, or mFD >1 mm, and regressed out Friston's 24 head-motion parameters (Friston et al. 1996) during the preprocessing steps (Yan et al. 2013). This procedure moderated the influence of head motion on the estimates of individual variability in the functional connectivity architecture. Furthermore, we conducted three separate analyses under more strict thresholds to validate our major findings.

For the variability analysis, we validated the effects of different window lengths, intra-subject variance, prematurity, temporal signal-to-noise ratio (tSNR), and unprocessed correlation matrix. (1) In the across-subject sliding window analysis, the optimal selection of window length remained unclear; thus, we considered two additional window lengths (8 infants and 12 infants) to validate the main results. (2) The intra-subject variance may be a confounding factor in the variability estimation. However, this parameter is difficult to assess because repeated scans are not available in the current study. To make the approach applicable, we split the data from one session into two halves to estimate the intra-subject variance (Mueller et al. 2015), followed by a regression analysis. (3) To further exclude the influence of prematurity on the estimation of individual variability in functional connectivity, we regressed out the effects of birth age for validation. (4) We calculated the relationship between age and the tSNR/mFD, as well as the relationship between variability values and the averaged tSNR/mFD to explore the possibility that the changes of individual variability with age were driven by the tSNR or head motion during data collection. Here, tSNR values were calculated for each infant within the mask in which the blood oxygenation level-dependent signal values were > 400 (Van Dijk et al. 2012). (5) The absolute operation may disrupt the continuity of the original functional

connectivity profiles; therefore, we also calculated the inter-subject variability of the original functional correlation matrix only after Fisher's r -to- z transformation and without using absolute values. For details, see the Supplementary Material.

Reproducibility Analysis

To determine the reproducibility of our results, we performed the following analyses using another independent imaging dataset from the developing Human Connectome Project (dHCP: <http://www.developingconnectome.org/project/>) (Supplementary Table S1). Considering that the publicly available dHCP dataset only included R-fMRI data in term infants, we validated the reproducibility of the spatial distribution of individual variability patterns only in the Term Group. In the dHCP dataset, forty term infants were scanned using multiband-MRI during natural sleep. After excluding the infants with head-motion displacement >5 mm, rotation $>5^\circ$, or mFD >1 mm, the imaging data from 15-term neonates (mean age: 39.2 weeks) were used for the variability analysis. The effects of head motion were further explored by performing the analysis on data from 10 infants (mean age: 39.0 weeks) with a stricter head-motion threshold (excluding displacement movement >3 mm, rotational movement $>3^\circ$, or mFD >1 mm). For details, see the Supplementary Material.

To calculate the individual variability of functional connectivity in term infants from the dHCP dataset, we estimated the individual functional connectivity matrix as follows. First, we defined a rough gray matter mask by combining the cortex and deep gray matter probability templates after thresholding with a value of 0.2. Using the predefined rough mask, we extracted the effective R-fMRI time series of all infants. The final gray matter mask ($N_{\text{voxel}} = 11698$) was generated by intersecting masks across infants. For each infant, the Pearson correlation coefficients between pairs of voxels were calculated within the predefined gray matter mask, resulting in an 11698×11698 matrix, which was preserved after Fisher's r -to- z transformation and absolute operation. Finally, for all fifteen infants, the variability map was calculated using Equation (1) (here $N_{\text{voxel}} = 11698$, $M = 15$). Additionally, we regenerated the variability maps using the data from infants using three separate analyses with different head-motion exclusion thresholds and scrubbing methods for head-motion corrections (Power et al. 2012). We wrapped the individual variability maps of the dHCP data into the 37-week infant template using non-linear registration and nearest neighbor interpolation approaches to compare the spatial similarity between the two independent term groups (dHCP data and our data). Then, we computed Pearson correlation coefficients for the individual values across voxels between the two maps in the same coordinate space.

Results

Development of Individual Variability of Functional Connectivity

Sliding Window Analysis

We obtained temporally continuous patterns of individual variability in the functional connectivity of infants across all time windows (Fig. 2). At ~ 33 weeks (Window 1: 33.4 ± 1.1 weeks), we observed lower variability in primary sensorimotor and visual areas and higher variability in association regions (Fig. 2A). This spatial pattern is generally similar to that observed in adult brains (Mueller et al. 2013), suggesting that the individual

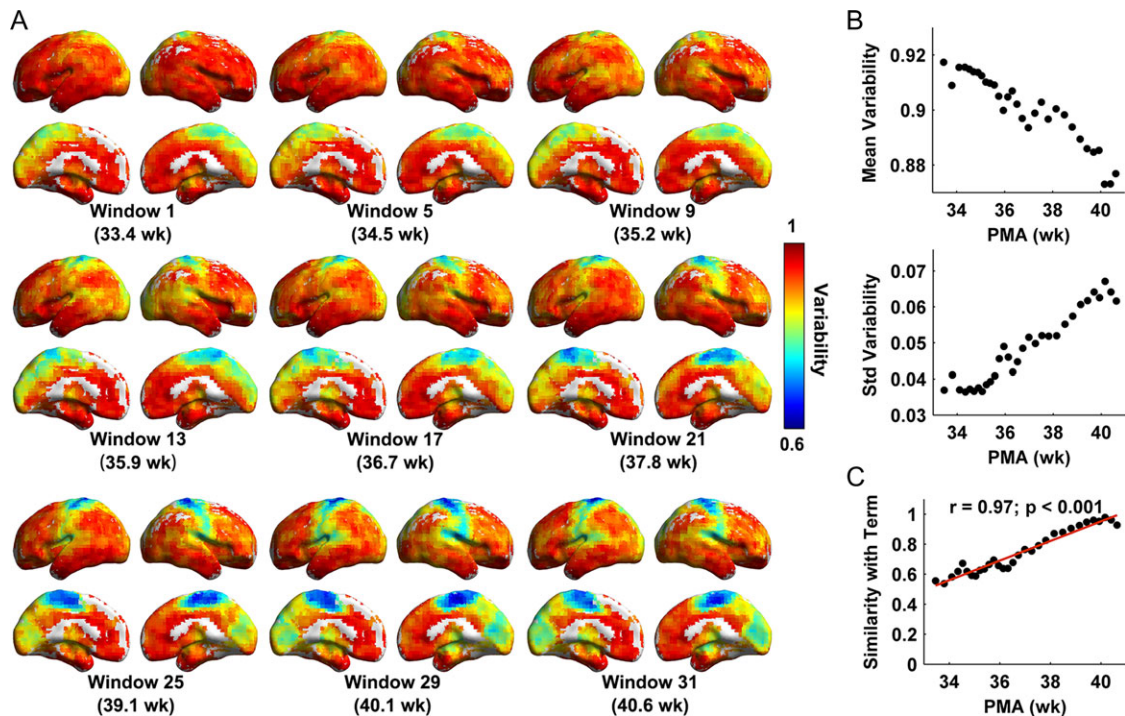


Figure 2. Results of the across-subject sliding window analysis of individual variability patterns in functional connectivity during the third trimester. (A) Spatial patterns of voxel-wise individual variability under each window age. (B) Continuous changes in variability of functional connectivity with the linearly decreasing global mean and the linearly increasing standard deviation. (C) The spatial similarity of individual variability maps between each window and term controls linearly increased with age ($r = 0.97$, $P < 0.001$). Values were mapped onto the cortical surface using BrainNet Viewer (Xia et al. 2013). PMA (weeks), postmenstrual age in weeks.

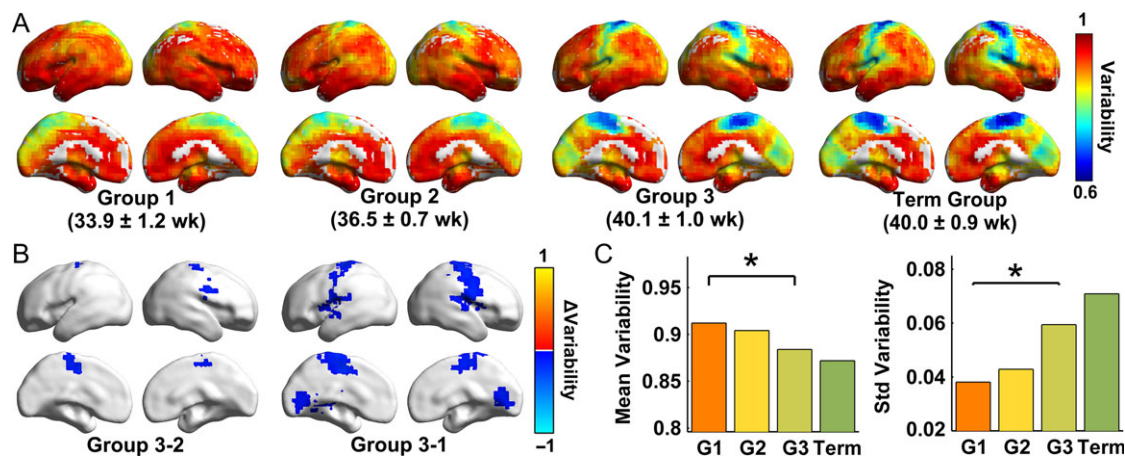


Figure 3. Results of the group-based statistical analysis of individual variability. (A) Individual variability maps of the voxel-wise functional connectivity in Group 1 (31.3–35.3 weeks), Group 2 (35.6–38.4 weeks), Group 3 (38.7–41.7 weeks), and the Term group (38.4–41 weeks). (B) The areas showing significant differences (voxel $P < 0.01$, cluster $P < 0.05$, cluster size $> 3\,726\text{ mm}^3$ for Group 3- Group 1, and cluster size $> 3\,510\text{ mm}^3$ for Group 3- Group 2, 10 000 permutations) in connectivity variability between groups. The blue clusters represent significant decreases detected by the permutation test. The values were mapped onto the cortical surface using BrainNet Viewer (Xia et al. 2013). (C) The means and standard deviations of individual variability values in the four age groups are shown. * $P < 0.05$, 10 000 permutations, Bonferroni corrected.

variability in the functional connectivity architecture of the brain has occurred by this stage. As development progressed, the variability values of the medial sensorimotor, occipital pole and lateral temporal regions decreased with age (Fig. 2A). At approximately the time of a normal birth (Window 31:40.6 ± 0.5 weeks), the individual variability pattern of the brain networks (Fig. 2A) was highly similar ($r = 0.93$, $P < 0.001$) to that of term control babies (40.0 ± 0.9 weeks) (Fig. 3A). Interestingly, the

mean variability of the whole brain decreased with development, whereas the standard deviation of variability increased (Fig. 2B). This observation implies that, although the global level of individual variability decreased, the heterogeneity of the individual variability across brain regions increased with age. Finally, the across-voxel spatial similarity of variability maps between each window and the term infant control group increased significantly with age ($r = 0.97$, $P < 0.001$, Fig. 2C).

Group-based statistical analysis

We obtained individual variability maps for the three age groups and the Term Group (Fig. 3A), as well as the group differences (Fig. 3B). Briefly, the variability values of Group 3 exhibited significant decreases in medial supplementary motor areas and the lateral precentral gyrus compared with those of Group 2 (Fig. 3B, voxel $P < 0.01$, cluster $P < 0.05$, and cluster size $>3510 \text{ mm}^3$, 10 000 permutations). Compared with Group 1, Group 3 showed significantly decreased variability values in the paracentral lobule, pre-/post-central gyrus, and visual regions (Fig. 3B, voxel $P < 0.01$, cluster $P < 0.05$, and cluster size $>3726 \text{ mm}^3$, 10 000 permutations). Furthermore, the global mean values of individual variability decreased significantly with age (Fig. 3C, Group 3- Group 2: $P = 0.05$, uncorrected; Group 3- Group 1: $P = 0.024$, Bonferroni corrected; 10 000 permutations); the standard deviation of the variability values increased significantly with age (Fig. 3C, Group 3- Group 2: $P = 0.02$, uncorrected; Group 3-Group 1: $P = 0.001$, Bonferroni corrected; 10 000 permutations). Moreover, we observed increasing spatial similarity between each of the three groups and the Term Group over the course of development ($r = 0.61$, $P < 0.001$ for the spatial correlation between Group 1 and the Term Group; $r = 0.70$, $P < 0.001$ for the spatial correlation between Group 2 and the Term Group; and $r = 0.97$, $P < 0.001$ for the spatial correlation between Group 3 and the Term Group). Notably, no significant differences in individual variability were observed between either Group 2 and Group 1 or the Term Group and Group 3.

Non-uniform Development of Individual Variability across Brain Systems

Sliding Window Analysis

Visual examination revealed distinct developmental curves of individual variability across different brain systems (Fig. 4A). The somatomotor system exhibited relatively low inter-subject variability, which decreased dramatically across windows, whereas the visual, subcortical, and dorsal and ventral attention networks demonstrated moderate variability that mainly decreased after around 38 weeks. Meanwhile, the default mode, frontoparietal and limbic networks consistently displayed high functional variability that showed little change with age.

Group-based Statistical Analysis

For each age group, the inter-subject variability values among eight systems were significantly different from each other, as identified by the Kruskal-Wallis H test (all $P < 0.001$). In all four groups, the variability values of primary systems (the somatomotor and visual systems) were consistently lower than those of the other six systems (Fig. 4B, $P < 0.001$, Bonferroni corrected). The attention systems (i.e., the dorsal and ventral attention networks) exhibited moderate variability values that were significantly lower than the values of the limbic, frontoparietal, default, and subcortical systems in Group 3 and the Term Group (Fig. 4B, $P < 0.001$, Bonferroni corrected). These findings indicated that the primary brain systems exhibited a relatively lower variability than the higher-order cognitive systems, regardless of the group considered. Finally, between-group comparison analyses revealed that only the somatomotor system exhibited significant age-related decreases with development (Group 2- Group 1: $P = 0.02$, uncorrected; Group 3-Group 2: $P < 0.01$, Bonferroni corrected; Group 3- Group 1: $P < 0.01$, Bonferroni corrected; 10 000 permutations, Fig. 4C).

Relationship between Individual Variability and Distance-Dependent Connectivity

Across-subject sliding window analysis revealed that both the number and strength of functional connections increased with age within each distance bin (Fig. 5A and B). Moreover, the variability exhibited strengthened correlations with both the number and strength of different anatomical-distance connections with age (Fig. 6). Goodness-of-fit was compared using Akaike's information criterion (AIC) for the regression model: linear and quadratic relationships. Of these relations, the quadratic relation was the best-fitting model for the enhanced negative correlation between variability and the number/strength of short-range connections with age, with the turning points located at postmenstrual ages of 35.5 and 35.6 weeks, respectively (Fig. 6A). The linear relation was the best-fitting model for the enhanced negative correlation between variability and the number/strength of middle-range connections with age (Fig. 6B). Finally, the quadratic relation was the best-fitting model for the increased positive correlation between variability and the number/strength of long-range connections with age, with the turning points located at postmenstrual ages of 35.5 and 35.6 weeks, respectively (Fig. 6C). Based on these findings, a brain node with more numerous and stronger short- and middle- range connections tends to exhibit lower individual variability, whereas long-range connections are associated with higher individual variability. This effect of distance on individual variability increased with age during early development. These results were further confirmed by group-based analyses (Supplementary Tables S2 and S3).

Validation Results

To test the reliability of our results, we evaluated the effects of different processing steps and variability analysis factors on our main findings, including different brain templates during spatial normalization (Supplementary Figs S1 and S2), global signal removal (Supplementary Fig. S3), head motion (Supplementary Fig. S4), sliding window sizes (Supplementary Figs S5 and S6), intra-subject variance (Supplementary Fig. S7), prematurity (Supplementary Fig. S8), and use of the original matrix (Supplementary Figs S9 and S10). Our main findings remained largely unchanged following the implementation of these strategies (for details, see the Supplementary Results and Supplementary Figs S1–S10).

Reproducibility Results

Visual examination indicated that the functional variability maps of 15-term babies from the dHCP data (mean age: 39.2 weeks) were generally similar to those obtained from our main analysis of 10-term babies (mean age: 40.0 weeks) (Fig. 7A). Specifically, we consistently observed lower individual variability in medial/lateral motor areas, moderate variability in medial occipital areas and higher variability in association regions. However, we also noticed that the two groups showed relatively distinct patterns in the parietal-temporal association area and the visual cortex, which may be due to different scanning parameters, scanning status and sample heterogeneity between the two datasets. Nonetheless, these two maps displayed a significant spatial correlation across all voxels (Fig. 7B, $r = 0.62$, $P < 0.001$). Using a scrubbing procedure and a stricter head-motion threshold (excluding the infants with displacements $>3 \text{ mm}$, rotation $>3^\circ$, or mFD $>1 \text{ mm}$), we still observed high spatial similarity between the dHCP dataset and our data (Supplementary Fig. S11, all $P < 0.001$). Together, these results

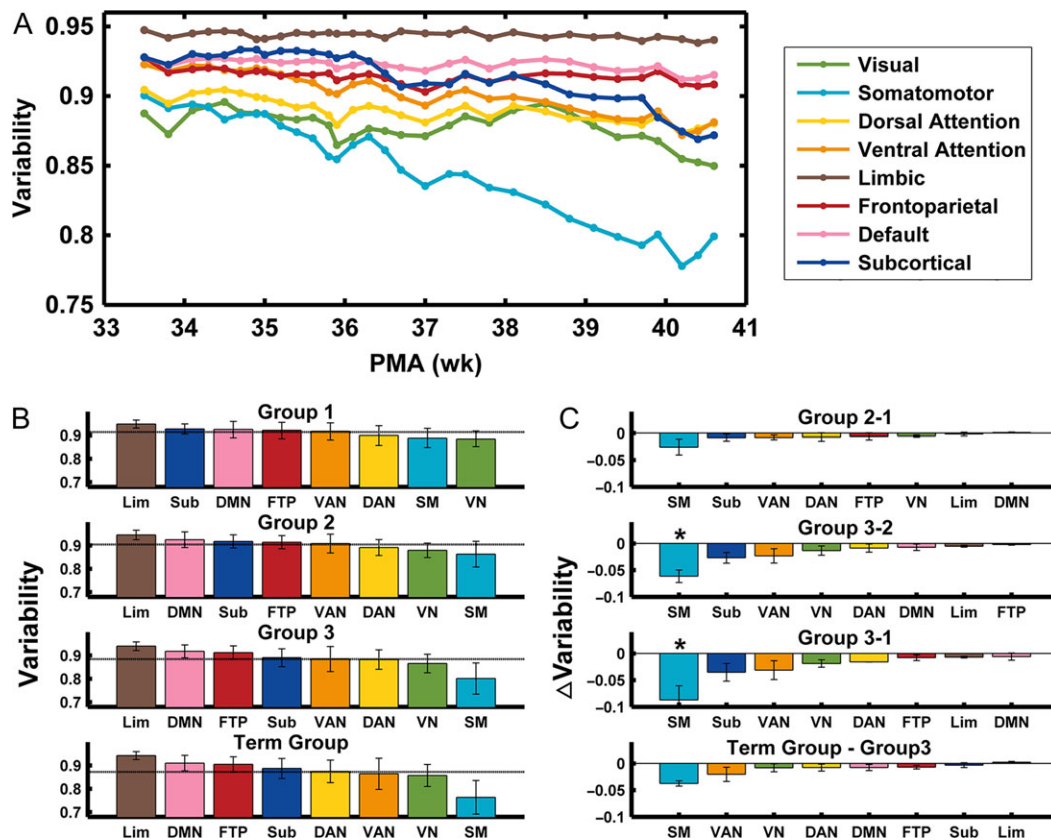


Figure 4. System-level individual variability changes during the third trimester. (A) Continuous changes in system-level individual variability of functional connectivity over the course of development, as revealed by the across-subject sliding window analysis. The differences of system-level individual variability within groups (B) and between groups (C) are shown. * $P < 0.05$, 10 000 permutations, Bonferroni corrected. PMA (weeks), postmenstrual age in weeks.

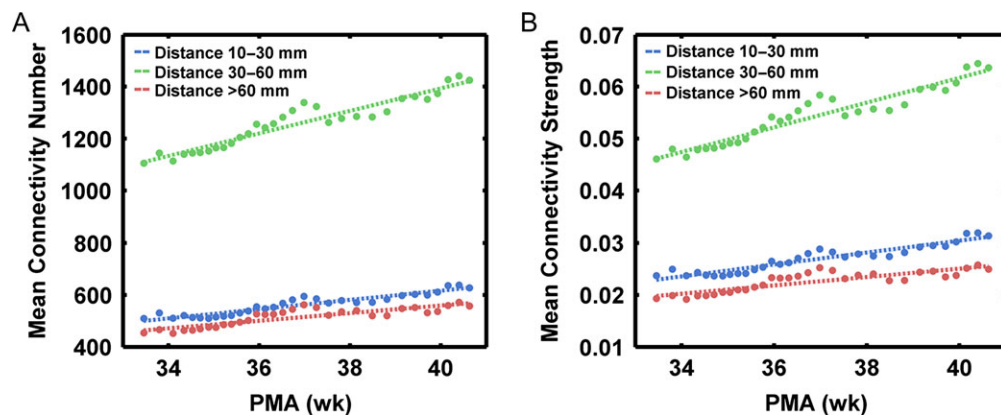


Figure 5. Across-subject sliding window analysis results reveal continuous changes in short-, middle-, long-range connectivity during the prenatal period. The mean number (A) and strength (B) of connections at different distances increase with age. PMA (weeks), postmenstrual age in weeks.

suggest high reproducibility in individual variability patterns between the datasets.

Discussion

Using R-fMRI data obtained from neonates aged ~31–42 postmenstrual weeks, we demonstrated the individual variability patterns of functional connectivity during prenatal brain development. Specifically, we observed lower individual variability in primary sensorimotor and visual areas and higher variability

in association areas, suggesting that individual variability patterns in the functional connectivity architecture have already emerged at approximately the beginning of the third trimester. Moreover, individual variability showed non-uniform changes across different brain systems, with dramatic decreases in the sensorimotor network, moderate decreases in the visual, dorsal and ventral attention and subcortical networks, and minimal changes in the default mode, frontoparietal and limbic networks. Finally, individual variability patterns were strongly correlated with the short- to middle-range connectivity and the

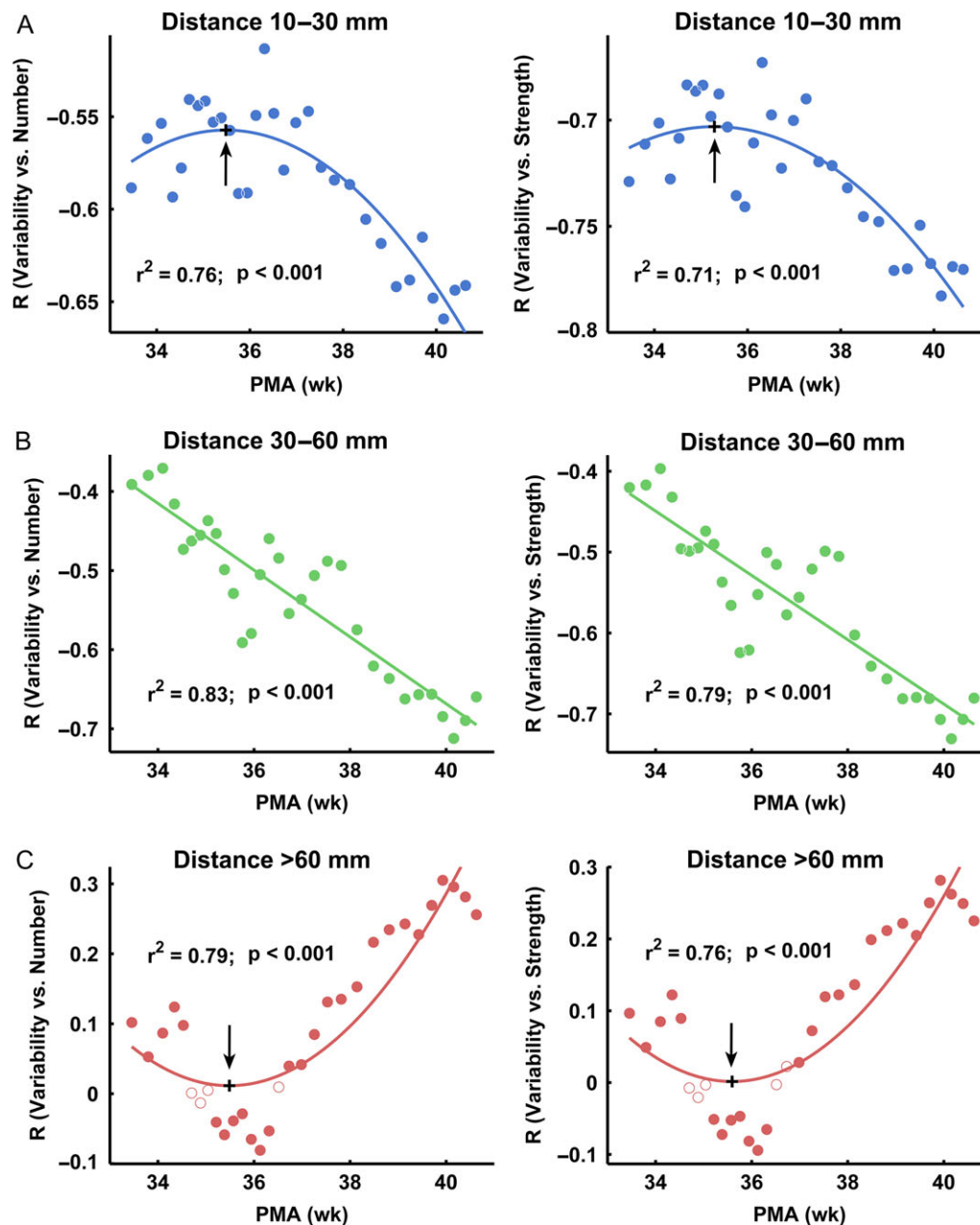


Figure 6. The relationships between individual variability and connectivity number/strength tend to be strengthened with development. (A) The quadratic relations between the variability and the number/strength (left/right panels) of short-range connections. (B) The linear relations between the variability and the number/strength (left/right panels) of middle-range connections. (C) The quadratic relations between the variability and the number/strength (left/right panels) of long-range connections. The black cross represents the turning point. The dot here represents the correlation values between variability and connectivity number/strength. The closed circles represent significant correlations ($P < 0.05$) and open circles represent non-significant correlations. PMA (weeks), postmenstrual age in weeks.

effects of the distance increased with age. Collectively, these findings highlight the developmental patterns of individual brain variability during the third trimester, providing insights into the network substrates underlying individual differences in cognition and behaviors later in life.

Spatial Distribution of Individual Variability of the Prenatal Brains

We observed relatively lower individual variability in the primary sensorimotor and visual regions and higher variability in the association cortex during the third trimester. This spatial

pattern was remarkably similar to that in both adults (Mueller et al. 2013) and neonates (Gao et al. 2014), suggesting that the adult-like individual variability is established during the prenatal phase. However, the overall variability values in the prenatal brain ($\sim 0.87\text{--}0.92$) were greater than those in neonates (~ 0.84) (Gao et al. 2014) and adults (~ 0.61) (Mueller et al. 2013), possibly due to the immature and relatively random state of the connectivity architecture of functional networks (Cao, He et al. 2017). Specifically, the limbic system, which showed lower variability in adults, ranked the highest in the eight systems and consistently demonstrated only limited changes during the prenatal period, which may be related to the lack of emotion

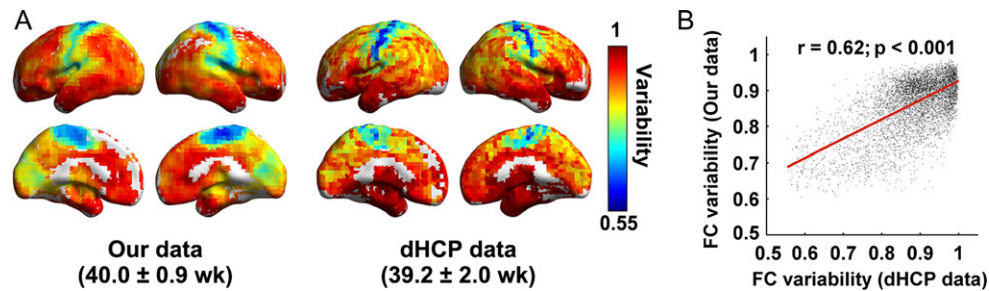


Figure 7. (A) The spatial patterns of individual variability in term infants from our dataset and the dHCP dataset. (B) A significant spatial correlation across voxels was identified between the two independent term groups ($r = 0.62$, $P < 0.001$).

and memory load before birth (Rifkin-Graboi et al. 2015). The default mode regions showed moderate individual variability in adults (Mueller et al. 2013) but exhibited high variability in neonates (Gao et al. 2014) and preterm babies in this study, perhaps due to the prolonged maturation of synchronization after birth (Gao et al. 2009, 2017). Meanwhile, the somatomotor and visual networks demonstrated lower variability values consistent with what is observed in adults, neonates (Mueller et al. 2013; Gao et al. 2014) and preterm babies. These lower values are mainly explained by the primary cortex developing prior to higher-order regions; focusing prenatal resources on the regions that are most important for early survival (Collin and van den Heuvel 2013; Cao, Huang et al. 2017). Interestingly, the variability in the right pre- and post-central areas exhibited lower values (Fig. 3A) and greater age-related variations (Fig. 3B) than the contralateral areas. This kind of asymmetric pattern was previously observed in structural development in neonates from 26 to 36 gestational weeks (Dubois et al. 2010) and one-month-old infants (Li et al. 2014). Here, we provided preliminary evidence for functional lateralization in the prenatal brain development.

It is interesting to discuss the mechanisms underlying individual variability during the third trimester. Previously, Mueller et al. (2013) suggested that the higher variability in association areas observed in adults is attributable to the relatively prolonged maturation in the presence of fruitful environmental factors and weaker genetic influences. However, this mechanism may be different from that in neonates (Gao et al. 2014) and preterm-born babies, considering the relatively limited exposure to the outside environment during early development. On the one hand, during the fetal and perinatal periods, the transient neuronal circuitry, which appears in the cerebral wall at the age of 8 weeks and disappears after the sixth post-natal month, underlies unique functions that may determine the developmental plasticity of the cerebral cortex and lead to the observed variability in infants (Kostović and Judaš 2006; Kostović et al. 2014). The growing projections and corticocortical pathways may also be engaged in transient connections, which show variable path lengths and are retracted or reorganized during peri- and post-natal development (Kostovic and Goldman-Rakic 1983; Kostovic and Jovanov-Milosevic 2006; Kostović and Judaš 2006; Kostović et al. 2014). Morphological research provides evidence for high structural variability in the association areas (particularly the prefrontal cortex) of adults and children (Rajkowska and Goldman-Rakic 1995). Neurons in layer III of the lateral prefrontal cortices rapidly increase from 27 to 32 weeks of gestation (Mrzljak et al. 1988). Around the same time, remarkable growth and refinement of connections in the association areas (e.g., prefrontal cortex) occurs and continues into post-natal periods (Kostovic and Goldman-Rakic

1983; Mrzljak et al. 1988, 1991, 1992; Zikopoulos and Barbas 2010; Kostović et al. 2014). This development is responsible for making the connectivity map variable across individuals. On the other hand, structural imaging studies have demonstrated genetic effects on nearly all white matter tracts in neonates (Lee et al. 2015) and minimal environmental effects on white matter development between twins and singletons during the first two years of life (Sadeghi et al. 2017). Functional imaging studies in 0- to 2-year-old infants also suggest that the environmental effects on the brain were fewer than the genetic effects (Gao et al. 2014). Therefore, we speculate that both neurogenesis and genetic influences are likely to contribute to the commonality and uniqueness of individual functional networks during prenatal development.

Age-related Changes in Individual Variability of Functional Networks during the Prenatal Phase

When exploring the effects of age on individual variability, the overall variability level decreased with development, with heterogeneous patterns for different regions. These variability decreases may be associated with the ordered developmental trajectory from random to well-organized structures (Cao, He et al. 2017). In this sense, the regional developmental heterogeneity was consistent with previous findings demonstrating the varying changing rates of the functional properties of different regions during this period (Cao, Huang et al. 2017; Keunen et al. 2017). Notably, the most rapid decreases appeared in the sensorimotor system, as its early establishment is vital for the early life of an infant (Buckner and Krienen 2013; Cao, Huang et al. 2017). More specifically, the medial primary sensorimotor areas showed lower variability during the whole third trimester, whereas the variability of the lateral sensorimotor areas was initially high and then decreased with age (Fig. 3A). By the time of birth, the medial and lateral primary areas all showed lower variability (Fig. 3A). Therefore, our findings indicated the medial-to-lateral development pattern of variability in the sensorimotor system, which is compatible with the order of development of interhemispheric connectivity (Smyser et al. 2010; Thomason et al. 2013). Notably, higher-order functional networks, such as the default mode and frontoparietal networks, showed high and unchanging variability values during this period, which were consistently reported as being immature in previous studies (Fransson et al. 2007; Smyser et al. 2010; Cao, He et al. 2017). Interestingly, the quantification of changes in cortical microstructural properties using diffusion MRI indicated a contrasting pattern, with the cortical microstructure of primary sensorimotor regions exhibiting the slowest changes and higher-order regions exhibiting the most rapid changes (Deipolyi et al. 2005; Yu et al. 2016).

Previous prenatal studies based on cellular-level analyses reported the differential timing of developmental events across regions in the transient subplate, where the somatosensory areas develop earlier than the visual regions (Kostovic and Rakic 1990; Tau and Peterson 2010). Lamination also occurs initially in the primary sensory and motor cortices at 25 weeks of gestation (Kostović et al. 1995). Synaptogenesis begins earlier in the primary motor area, and later in the prefrontal cortex (Huttenlocher 1984, 1990; Huttenlocher and Dabholkar 1997; Tau and Peterson 2010). The global pattern of the progression of white matter myelination follows a caudal-to-rostral gradient and central-to-peripheral order (Qiu et al. 2015). Moreover, a histological study of neonatal brains revealed the presence of granular layer IV in all neocortical areas, in which the primary cortical areas are identified based on their cytoarchitecture, whereas association cortices are less clearly delineated (Kostovic and Rakic 1980). These cellular-level processes are believed to establish the fundamental anatomical organization for the initial function of neural circuits (Tau and Peterson 2010). Thus, our findings at the systems level are consistent with these cellular-level speculations. Notably, the variability value of the subcortical system was the second highest in very preterm babies but rapidly decreased with age (Figs. 4A and B), possibly because the subcortical areas undergo a period of extensive development during the prenatal period, strengthening their intra- and to-cortical connections (Tau and Peterson 2010; Thomason et al. 2015; Toulmin et al. 2015). Additionally, matured myelin is first detected in subcortical regions between 20 and 28 weeks of gestation, followed by cortical regions including the precentral and post-central gyri and the optic radiation at 35 weeks of gestation (Iai et al. 1997). Collectively, our studies provide critical evidence for the medial-to-lateral and the primary-to-higher-order maturation trajectories during the third trimester from the perspective of inter-subject connectivity variability.

Distance Constraints on Individual Variability Enhanced with Development

Human brain networks exhibit a complex architecture with highly specialized local areas and sparsely linked distant areas for efficient information segregation and integration processing (Achard and Bullmore 2007; Bullmore and Sporns 2012; van den Heuvel and Sporns 2013; Liao, Vasilakos et al. 2017). Functional variability in neonates and adults positively correlates with the degree of long-range connectivity but negatively correlates with local connectivity (Mueller et al. 2013; Wang and Liu 2014). Thus, the relatively uniform and rich local connectivity may be associated with limited functional variability, whereas high functional variability may be induced by the emergence of distant connectivity for global information integration. Indeed, we observed negative correlations between variability values and both the numbers/strength of short- to middle-range connections, as well as positive correlations between variability values and the number/strength of long-range connections. This finding implied that the distance constraint on inter-subject variability is established before birth. Moreover, short- to middle-range connections predominantly develop during the third trimester (Cao, He et al. 2017), which may account for the rapid decrease in individual variability observed in the present study.

It is important to note that the strength of both the negative and positive correlations between variability and short- and long-range connectivity significantly improved with age during the third trimester. Previously, these distance effects on brain

connectivity have been reported in infants aged 0–2 years (Gao et al. 2014). During the prenatal period, the brain's functional networks are relatively immature (Fransson et al. 2011; Smyser et al. 2011), and distance-dependent connectivity in brain networks rapidly develops with age (Cao et al. 2016; Cao, He et al. 2017; Toth et al. 2017). Specifically, we observed that the negative correlation between variability and short-range connectivity was rapidly enhanced after 36 weeks. Moreover, the turning point for the positive correlation between variability and long-range connectivity with age was also observed at approximately 36 weeks. This result is supported by a previous MRI study in which the proportion of myelinated white matter in the whole brain increased from 1% to 5% between 36 and 40 gestational weeks (Hüppi et al. 1998). Based on these previous findings and our results, a gestational age of 36 weeks could be considered an important turning point during the prenatal development. Taken together, the increased distance constraint on inter-subject connectivity variability may result from the improved functional status of these connections.

Limitations, Technical Considerations, and Future Directions

Several issues need to be addressed. First, preterm birth represents a major risk factor for the potentially adverse development of functional connectivity (Smyser et al. 2010; Kwon et al. 2015; Cao, Huang et al. 2017). Currently, examination of preterm-born babies is widely used to depict developmental trajectories of the human brain during the third trimester (Fransson et al. 2007; Doria et al. 2010; Smyser et al. 2010). Considering that the dramatic developmental factor during the prenatal phase is very likely to exceed more the subtle preterm effects (Bourgeois et al. 1989; Kostovic 1990), we cannot exclude the possibility that the observed variability in development may be affected by exposure to the extrauterine environment. Our results could be further confirmed using the rapidly advancing fetal imaging technologies, which can depict longitudinal brain developmental trajectories in utero (van den Heuvel and Thomason 2016). Second, considering the potential bias of head motion on our results, we processed the R-fMRI data with Friston's 24-parameter regression (Friston et al. 1996) to reduce the confounding influence of motion artifacts. Moreover, our main findings exhibited little change under different head-motion exclusion thresholds and correction approaches. Thus, our results in variability were not attributable to head-motion artifacts. Third, given that global signal removal is still a debatable practice for physiological interpretations (Murphy and Fox 2017), we did not regress out the global signal in our main analyses. The validation analysis using the preprocessed data with global signal removal yielded similar age-related decreases in individual variability in all regions except for the visual cortex (Fig. S3E). Specifically, global signal regression has been shown to partly reduce functional correlations involving visual regions (Murphy et al. 2009; Chai et al. 2012; Cao, He et al. 2017). Previous R-fMRI studies on adults have shown that the use of different acquisition parameters and preprocessing methods affect the measurement of individual differences (Airan et al. 2016; Geerligs et al. 2017), further studies are required to explore whether these factors jointly affect the inter-individual differences in infants. Fourth, the brain parcellation that we used for functional system variability analysis was derived from an adult system parcellation using approximately 1000 subjects (Yeo et al. 2011) because of the lack of a specific infant system parcellation. Although this approach has been widely used in studies of early brain development (Gao et al. 2014, 2015), we do

recognize that future studies aiming to depict infant-specific system parcellation are urgently needed because of the immature functional and structural properties of infants compared with adults. Fifth, the different sleep states among infants may introduce bias in the findings regarding individual variability (Cao, Huang et al. 2017; Gao et al. 2017). In the present study, all infants were well-fed and imaged as soon as possible after they fell asleep; we assumed that this procedure would largely ensure little variation in sleep states among the infants. Finally, an increasingly common view is that mapping functional signals onto cortical surfaces to leverage surface-based registration and smoothing may lead to significantly better studies of brain functional connectivity. Currently, some well-developed surface-based registration pipelines are available for adults and infants at term age (Glasser et al. 2013; Li et al. 2015). However, surface-based studies on prenatal brain development remained rare because of the difficulty in image segmentation caused by the immature anatomical structure.

In conclusion, our findings highlight the developmental patterns of individual variability in the functional connectivity architecture during the third trimester. Future evaluations of the relationship between individual variability in the functional connectivity architecture during the prenatal development and individual cognition and behavioral differences later in life are still needed.

Supplementary Material

Supplementary material is available at *Cerebral Cortex* online.

Funding

This work was supported by the Changjiang Scholar Professorship Award (Award no. T2015027), the Natural Science Foundation of China (Grant nos 31830034, 81620108016, 81628009, 31521063), Beijing Natural Science Foundation (Grant Nos Z161100004916027 and Z151100003915082), the National Institutes of Health (NIH) of the United States (MH092535, MH092535-S1), the China Postdoctoral Science Foundation (Grant no. 2016M600955), the Open Research Fund of the State Key Laboratory of Cognitive Neuroscience and Learning (Grant no. CNLYB1407 to Y.H. and H.H.) and the Fundamental Research Funds for the Central Universities (Grant no. 2017XTCX04). Part of the results in validation analysis were obtained using data made available from the Developing Human Connectome Project funded by the European Research Council under the European Union's Seventh Framework Programme (FP/2007-2013)/(ERC Grant Agreement no. 319456).

Notes

We thank the lab member, Michelle Slinger, for assistance in English editing. *Conflict of Interest*: None declared.

References

Achard S, Bullmore E. 2007. Efficiency and cost of economical brain functional networks. *PLoS Comput Biol*. 3:e17.
 Airan RD, Vogelstein JT, Pillai JJ, Caffo B, Pekar JJ, Sair HI. 2016. Factors affecting characterization and localization of inter-individual differences in functional connectivity using MRI. *Hum Brain Mapp*. 37:1986–1997.
 Amunts K, Kedo O, Kindler M, Pieperhoff P, Mohlberg H, Shah NJ, Habel U, Schneider F, Zilles K. 2005. Cytoarchitectonic mapping of the human amygdala, hippocampal region and

entorhinal cortex: intersubject variability and probability maps. *Anat Embryol (Berl)*. 210:343–352.
 Amunts K, Weiss PH, Mohlberg H, Pieperhoff P, Eickhoff S, Gurd JM, Marshall JC, Shah NJ, Fink GR, Zilles K. 2004. Analysis of neural mechanisms underlying verbal fluency in cytoarchitectonically defined stereotaxic space - The roles of Brodmann areas 44 and 45. *Neuroimage*. 22:42–56.
 Baldassarre A, Lewis CM, Committeri G, Snyder AZ, Romani GL, Corbetta M. 2012. Individual variability in functional connectivity predicts performance of a perceptual task. *Proc Natl Acad Sci USA*. 109:3516–3521.
 Biswal B, Yetkin FZ, Haughton VM, Hyde JS. 1995. Functional connectivity in the motor cortex of resting human brain using echo-planar MRI. *Magn Reson Med*. 34:537–541.
 Bourgeois JP, Jastreboff PJ, Rakic P. 1989. Synaptogenesis in visual cortex of normal and preterm monkeys: evidence for intrinsic regulation of synaptic overproduction. *Proc Natl Acad Sci USA*. 86:4297–4301.
 Buckner RL, Krienen FM. 2013. The evolution of distributed association networks in the human brain. *Trends Cogn Sci*. 17:648–665.
 Bullmore E, Sporns O. 2012. The economy of brain network organization. *Nat Rev Neurosci*. 13:336–349.
 Bystron I, Blakemore C, Rakic P. 2008. Development of the human cerebral cortex: Boulder Committee revisited. *Nat Rev Neurosci*. 9:110–122.
 Cao M, He Y, Dai Z, Liao X, Jeon T, Ouyang M, Chalak L, Bi Y, Rollins N, Dong Q, et al. 2017. Early development of functional network segregation revealed by connectomic analysis of the preterm human brain. *Cereb Cortex*. 27:1949–1963.
 Cao M, Huang H, He Y. 2017. Developmental connectomics from infancy through early childhood. *Trends Neurosci*. 40:494–506.
 Cao M, Huang H, Peng Y, Dong Q, He Y. 2016. Toward developmental connectomics of the human brain. *Front Neuroanat*. 10:25.
 Chai XJ, Castañón AN, Öngür D, Whitfield-Gabrieli S. 2012. Anticorrelations in resting state networks without global signal regression. *Neuroimage*. 59:1420–1428.
 Chen CH, Gutierrez ED, Thompson W, Panizzon MS, Jernigan TL, Eyster LT, Fennema-Notestine C, Jak AJ, Neale MC, Franz CE, et al. 2012. Hierarchical genetic organization of human cortical surface area. *Science*. 335:1634–1636.
 Collin G, van den Heuvel MP. 2013. The ontogeny of the human connectome: development and dynamic changes of brain connectivity across the life span. *Neuroscientist*. 19:616–628.
 Dehaene-Lambertz G, Spelke ES. 2015. The infancy of the human brain. *Neuron*. 88:93–109.
 Deipolyi AR, Mukherjee P, Gill K, Henry RG, Partridge SC, Veeraraghavan S, Jin H, Lu Y, Miller SP, Ferriero DM, et al. 2005. Comparing microstructural and macrostructural development of the cerebral cortex in premature newborns: diffusion tensor imaging versus cortical gyration. *Neuroimage*. 27:579–586.
 Doria V, Beckmann CF, Arichi T, Merchant N, Groppo M, Turkheimer FE, Counsell SJ, Murgasova M, Aljabar P, Nunes RG, et al. 2010. Emergence of resting state networks in the preterm human brain. *Proc Natl Acad Sci USA*. 107:20015–20020.
 Dubois J, Benders M, Lazeyras F, Borradori-Tolsa C, Leuchter RH, Mangin JF, Huppi PS. 2010. Structural asymmetries of perisylvian regions in the preterm newborn. *Neuroimage*. 52:32–42.
 Feng L, Li H, Oishi K, Mishra V, Song L, Peng Q, Ouyang M, Wang J, Slinger M, Jeon T, et al. 2018. Age-specific gray and

- white matter DTI atlas for human brain at 33, 36 and 39 postmenstrual weeks. *Neuroimage*. doi:10.1016/j.neuroimage.2018.06.069.
- Finn ES, Shen X, Scheinost D, Rosenberg MD, Huang J, Chun MM, Papademetris X, Constable RT. 2015. Functional connectome fingerprinting: identifying individuals using patterns of brain connectivity. *Nat Neurosci*. 18:1664–1671.
- Fox MD, Snyder AZ, Vincent JL, Corbetta M, Van Essen DC, Raichle ME. 2005. The human brain is intrinsically organized into dynamic, anticorrelated functional networks. *Proc Natl Acad Sci USA*. 102:9673–9678.
- Fransson P, Aden U, Blennow M, Lagercrantz H. 2011. The functional architecture of the infant brain as revealed by resting-state fMRI. *Cereb Cortex*. 21:145–154.
- Fransson P, Skiold B, Horsch S, Nordell A, Blennow M, Lagercrantz H, Aden U. 2007. Resting-state networks in the infant brain. *Proc Natl Acad Sci USA*. 104:15531–15536.
- Friston KJ, Williams S, Howard R, Frackowiak RS, Turner R. 1996. Movement-related effects in fMRI time-series. *Magn Reson Med*. 35:346–355.
- Frost MA, Goebel R. 2012. Measuring structural-functional correspondence: spatial variability of specialised brain regions after macro-anatomical alignment. *Neuroimage*. 59:1369–1381.
- Gao W, Alcauter S, Smith JK, Gilmore JH, Lin W. 2015. Development of human brain cortical network architecture during infancy. *Brain Struct Funct*. 220:1173–1186.
- Gao W, Elton A, Zhu H, Alcauter S, Smith JK, Gilmore JH, Lin W. 2014. Intersubject variability of and genetic effects on the brain's functional connectivity during infancy. *J Neurosci*. 34:11288–11296.
- Gao W, Lin W, Grewen K, Gilmore JH. 2017. Functional connectivity of the infant human brain: plastic and modifiable. *Neuroscientist*. 23:169–184.
- Gao W, Zhu H, Giovanello KS, Smith JK, Shen D, Gilmore JH, Lin W. 2009. Evidence on the emergence of the brain's default network from 2-week-old to 2-year-old healthy pediatric subjects. *Proc Natl Acad Sci USA*. 106:6790–6795.
- Geerligs L, Tsvetanov KA, Cam C, Henson RN. 2017. Challenges in measuring individual differences in functional connectivity using fMRI: the case of healthy aging. *Hum Brain Mapp*. 38:4125–4156.
- Glasser MF, Sotiropoulos SN, Wilson JA, Coalson TS, Fischl B, Andersson JL, Xu J, Jbabdi S, Webster M, Polimeni JR, et al, Consortium WU-MH. 2013. The minimal preprocessing pipelines for the human connectome project. *Neuroimage*. 80:105–124.
- Good CD, Johnsrude IS, Ashburner J, Henson RN, Friston KJ, Frackowiak RS. 2001. A voxel-based morphometric study of ageing in 465 normal adult human brains. *Neuroimage*. 14:21–36.
- Hill J, Inder T, Neil J, Dierker D, Harwell J, Van Essen D. 2010. Similar patterns of cortical expansion during human development and evolution. *Proc Natl Acad Sci USA*. 107:13135–13140.
- Hüppi PS, Warfield S, Kikinis R, Barnes PD, Zientara GP, Jolesz FA, Tsuji MK, Volpe JJ. 1998. Quantitative magnetic resonance imaging of brain development in premature and mature newborns. *Ann Neurol*. 43:224–235.
- Huttenlocher PR. 1984. Synapse elimination and plasticity in developing human cerebral cortex. *Am J Ment Defic*. 88:488–496.
- Huttenlocher PR. 1990. Morphometric study of human cerebral cortex development. *Neuropsychologia*. 28:517–527.
- Huttenlocher PR, Dabholkar AS. 1997. Regional differences in synaptogenesis in human cerebral cortex. *J Comp Neurol*. 387:167–178.
- Iai M, Yamamura T, Takashima S. 1997. Early expression of proteolipid protein in human fetal and infantile cerebri. *Pediatr Neurol*. 17:235–239.
- Kanai R, Rees G. 2011. The structural basis of inter-individual differences in human behaviour and cognition. *Nat Rev Neurosci*. 12:231–242.
- Keunen K, Counsell SJ, Benders M. 2017. The emergence of functional architecture during early brain development. *Neuroimage*. 160:2–14.
- Kostovic I. 1990. Structural and histochemical reorganization of the human prefrontal cortex during perinatal and postnatal life. *Prog Brain Res*. 85:223–239. discussion 239–240.
- Kostovic I, Goldman-Rakic PS. 1983. Transient cholinesterase staining in the mediodorsal nucleus of the thalamus and its connections in the developing human and monkey brain. *J Comp Neurol*. 219:431–447.
- Kostovic I, Jovanov-Milosevic N. 2006. The development of cerebral connections during the first 20-45 weeks' gestation. *Semin Fetal Neonatal Med*. 11:415–422.
- Kostović I, Jovanov-Milošević N, Radoš M, Sedmak G, Benjak V, Kostović-Srzić M, Vasung L, Čuljat M, Radoš M, Hüppi P. 2014. Perinatal and early postnatal reorganization of the subplate and related cellular compartments in the human cerebral wall as revealed by histological and MRI approaches. *Brain Struct Funct*. 219:231–253.
- Kostović I, Judaš M. 2006. Prolonged coexistence of transient and permanent circuitry elements in the developing cerebral cortex of fetuses and preterm infants. *Dev Med Child Neurol*. 48:388–393.
- Kostović I, Judaš M, Petanjek Z, Šimić G. 1995. Ontogenesis of goal-directed behavior: anatomo-functional considerations. *Int J Psychophysiol*. 19:85–102.
- Kostovic I, Rakic P. 1980. Cytology and time of origin of interstitial neurons in the white matter in infant and adult human and monkey telencephalon. *J Neurocytol*. 9:219–242.
- Kostovic I, Rakic P. 1990. Developmental history of the transient subplate zone in the visual and somatosensory cortex of the macaque monkey and human brain. *J Comp Neurol*. 297:441–470.
- Kwon SH, Scheinost D, Lacadie C, Sze G, Schneider KC, Dai F, Constable RT, Ment LR. 2015. Adaptive mechanisms of developing brain: cerebral lateralization in the prematurely-born. *Neuroimage*. 108:144–150.
- Lee SJ, Steiner RJ, Luo S, Neale MC, Styner M, Zhu H, Gilmore JH. 2015. Quantitative tract-based white matter heritability in twin neonates. *Neuroimage*. 111:123–135.
- Li G, Nie J, Wang L, Shi F, Lyall AE, Lin W, Gilmore JH, Shen D. 2014. Mapping longitudinal hemispheric structural asymmetries of the human cerebral cortex from birth to 2 years of age. *Cereb Cortex*. 24:1289–1300.
- Li G, Wang L, Shi F, Gilmore JH, Lin W, Shen D. 2015. Construction of 4D high-definition cortical surface atlases of infants: Methods and applications. *Med Image Anal*. 25:22–36.
- Liao X, Cao M, Xia M, He Y. 2017. Individual differences and time-varying features of modular brain architecture. *Neuroimage*. 152:94–107.
- Liao X, Vasilakos AV, He Y. 2017. Small-world human brain networks: perspectives and challenges. *Neurosci Biobehav Rev*. 77:286–300.
- Liu J, Liao XH, Xia MR, He Y. 2018. Chronnectome fingerprinting: identifying individuals and predicting higher cognitive functions using dynamic brain connectivity patterns. *Hum Brain Mapp*. 39:902–915.

- Liu J, Xia M, Dai Z, Wang X, Liao X, Bi Y, He Y. 2017. Intrinsic brain hub connectivity underlies individual differences in spatial working memory. *Cereb Cortex*. 27:5496–5508.
- Makropoulos A, Aljabar P, Wright R, Huning B, Merchant N, Arichi T, Tumor N, Hajnal JV, Edwards AD, Counsell SJ, et al. 2016. Regional growth and atlas of the developing human brain. *Neuroimage*. 125:456–478.
- Molliver ME, Kostovic I, van der Loos H. 1973. The development of synapses in cerebral cortex of the human fetus. *Brain Res*. 50:403–407.
- Mrzljak L, Uylings HB, Kostovic I, Van Eden CG. 1988. Prenatal development of neurons in the human prefrontal cortex: I. A qualitative Golgi study. *J Comp Neurol*. 271:355–386.
- Mrzljak L, Uylings HB, Kostovic I, van Eden CG. 1992. Prenatal development of neurons in the human prefrontal cortex. II. A quantitative Golgi study. *J Comp Neurol*. 316:485–496.
- Mrzljak L, Uylings HB, Van Eden GG, Judáš M. 1991. Neuronal development in human prefrontal cortex in prenatal and postnatal stages. *Prog Brain Res*. 85:185–222. Elsevier.
- Mueller S, Wang D, Fox MD, Pan R, Lu J, Li K, Sun W, Buckner RL, Liu H. 2015. Reliability correction for functional connectivity: theory and implementation. *Hum Brain Mapp*. 36:4664–4680.
- Mueller S, Wang D, Fox MD, Yeo BT, Sepulcre J, Sabuncu MR, Shafee R, Lu J, Liu H. 2013. Individual variability in functional connectivity architecture of the human brain. *Neuron*. 77:586–595.
- Murphy K, Birn RM, Handwerker DA, Jones TB, Bandettini PA. 2009. The impact of global signal regression on resting state correlations: are anti-correlated networks introduced? *Neuroimage*. 44:893–905.
- Murphy K, Fox MD. 2017. Towards a consensus regarding global signal regression for resting state functional connectivity MRI. *Neuroimage*. 154:169–173.
- Ouyang M, Liu P, Jeon T, Chalak L, Heyne R, Rollins NK, Licht DJ, Detre JA, Roberts T, Lu H, Huang H, 2017. Heterogeneous increases of regional cerebral blood flow during preterm brain development: Preliminary assessment with pseudo-continuous arterial spin labeled perfusion MRI. *Neuroimage*. 147:233–242.
- Petanjek Z, Judas M, Simic G, Rasin MR, Uylings HB, Rakic P, Kostovic I. 2011. Extraordinary neoteny of synaptic spines in the human prefrontal cortex. *Proc Natl Acad Sci USA*. 108:13281–13286.
- Power JD, Barnes KA, Snyder AZ, Schlaggar BL, Petersen SE. 2012. Spurious but systematic correlations in functional connectivity MRI networks arise from subject motion. *Neuroimage*. 59:2142–2154.
- Power JD, Mitra A, Laumann TO, Snyder AZ, Schlaggar BL, Petersen SE. 2014. Methods to detect, characterize, and remove motion artifact in resting state fMRI. *Neuroimage*. 84:320–341.
- Power JD, Plitt M, Laumann TO, Martin A. 2017. Sources and implications of whole-brain fMRI signals in humans. *Neuroimage*. 146:609–625.
- Qiu A, Mori S, Miller MI. 2015. Diffusion tensor imaging for understanding brain development in early life. *Annu Rev Psychol*. 66:853–876.
- Rajkowska G, Goldman-Rakic PS. 1995. Cytoarchitectonic definition of prefrontal areas in the normal human cortex: II. Variability in locations of areas 9 and 46 and relationship to the Talairach Coordinate System. *Cereb Cortex*. 5:323–337.
- Rakic P. 1972. Mode of cell migration to the superficial layers of fetal monkey neocortex. *J Comp Neurol*. 145:61–83.
- Rakic P. 1995. Radial versus tangential migration of neuronal clones in the developing cerebral cortex. *Proc Natl Acad Sci USA*. 92:11323–11327.
- Rifkin-Graboi A, Kong L, Sim LW, Sanmugam S, Broekman BF, Chen H, Wong E, Kwek K, Saw SM, Chong YS, et al. 2015. Maternal sensitivity, infant limbic structure volume and functional connectivity: a preliminary study. *Transl Psychiatry*. 5:e668.
- Sadeghi N, Gilmore JH, Gerig G. 2017. Twin-singleton developmental study of brain white matter anatomy. *Hum Brain Mapp*. 38:1009–1024.
- Satterthwaite TD, Elliott MA, Gerraty RT, Ruparel K, Loughhead J, Calkins ME, Eickhoff SB, Hakonarson H, Gur RC, Gur RE, et al. 2013. An improved framework for confound regression and filtering for control of motion artifact in the preprocessing of resting-state functional connectivity data. *Neuroimage*. 64:240–256.
- Serag A, Aljabar P, Ball G, Counsell SJ, Boardman JP, Rutherford MA, Edwards AD, Hajnal JV, Rueckert D. 2012. Construction of a consistent high-definition spatio-temporal atlas of the developing brain using adaptive kernel regression. *Neuroimage*. 59:2255–2265.
- Shen XL, Finn ES, Scheinost D, Rosenberg MD, Chun MM, Papademetris X, Constable RT. 2017. Using connectome-based predictive modeling to predict individual behavior from brain connectivity. *Nat Protoc*. 12:506–518.
- Sidman RL, Rakic P. 1973. Neuronal migration, with special reference to developing human brain: a review. *Brain Res*. 62:1–35.
- Smith SM, Vidaurre D, Beckmann CF, Glasser MF, Jenkinson M, Miller KL, Nichols TE, Robinson EC, Salimi-Khorshidi G, Woolrich MW, et al. 2013. Functional connectomics from resting-state fMRI. *Trends Cogn Sci*. 17:666–682.
- Smyser CD, Inder TE, Shimony JS, Hill JE, Degnan AJ, Snyder AZ, Neil JJ. 2010. Longitudinal analysis of neural network development in preterm infants. *Cereb Cortex*. 20:2852–2862.
- Smyser CD, Snyder AZ, Neil JJ. 2011. Functional connectivity MRI in infants: exploration of the functional organization of the developing brain. *Neuroimage*. 56:1437–1452.
- Tau GZ, Peterson BS. 2010. Normal development of brain circuits. *Neuropsychopharmacology*. 35:147–168.
- Thomason ME, Dassanayake MT, Shen S, Katkuri Y, Alexis M, Anderson AL, Yeo L, Mody S, Hernandez-Andrade E, Hassan SS, et al. 2013. Cross-hemispheric functional connectivity in the human fetal brain. *Sci Transl Med*. 5:173ra124.
- Thomason ME, Grove LE, Lozon TA Jr., Vila AM, Ye Y, Nye MJ, Manning JH, Pappas A, Hernandez-Andrade E, Yeo L, et al. 2015. Age-related increases in long-range connectivity in fetal functional neural connectivity networks in utero. *Dev Cogn Neurosci*. 11:96–104.
- Toth B, Urban G, Haden GP, Mark M, Torok M, Stam CJ, Winkler I. 2017. Large-scale network organization of EEG functional connectivity in newborn infants. *Hum Brain Mapp*. 38:4019–4033.
- Toulmin H, Beckmann CF, O’Muircheartaigh J, Ball G, Nongena P, Makropoulos A, Ederies A, Counsell SJ, Kennea N, Arichi T, et al. 2015. Specialization and integration of functional thalamocortical connectivity in the human infant. *Proc Natl Acad Sci USA*. 112:6485–6490.
- van den Heuvel MP, Sporns O. 2013. Network hubs in the human brain. *Trends Cogn Sci*. 17:683–696.
- van den Heuvel MI, Thomason ME. 2016. Functional connectivity of the human brain *in utero*. *Trends Cogn Sci*. 20:931–939.
- Van Dijk KR, Sabuncu MR, Buckner RL. 2012. The influence of head motion on intrinsic functional connectivity MRI. *Neuroimage*. 59:431–438.

- Wang D, Liu H. 2014. Functional connectivity architecture of the human brain: not all the same. *Neuroscientist*. 20:432–438.
- Xia M, Wang J, He Y. 2013. BrainNet viewer: a network visualization tool for human brain connectomics. *PLoS One*. 8: e68910.
- Yan CG, Craddock RC, He Y, Milham MP. 2013. Addressing head motion dependencies for small-world topologies in functional connectomics. *Front Hum Neurosci*. 7:910.
- Yan C-G, Zang Y-F. 2010. DPARSF: a MATLAB toolbox for “Pipeline” data analysis of resting-state fMRI. *Front Syst Neurosci*. 4:13.
- Yeo BT, Krienen FM, Sepulcre J, Sabuncu MR, Lashkari D, Hollinshead M, Roffman JL, Smoller JW, Zollei L, Polimeni JR, et al. 2011. The organization of the human cerebral cortex estimated by intrinsic functional connectivity. *J Neurophysiol*. 106:1125–1165.
- Yu Q, Ouyang A, Chalak L, Jeon T, Chia J, Mishra V, Sivarajan M, Jackson G, Rollins N, Liu S, et al. 2016. Structural development of human fetal and preterm brain cortical plate based on population-averaged templates. *Cereb Cortex*. 26:4381–4391.
- Zikopoulos B, Barbas H. 2010. Changes in prefrontal axons may disrupt the network in autism. *J Neurosci*. 30:14595–14609.